Effect of a density isomer on high-energy heavy-ion collisions

J. R. Nix and D. Strottman
Theoretical Division, Los Alamos Scientific Laboratory, Los Alamos, New Mexico 87545
(Received 25 July 1980)

On the basis of conventional nuclear fluid dynamics, we study the sensitivity of high-energy heavy-ion collisions to a density isomer in the nuclear equation of state, as well as to a variation in the nuclear compressibility coefficient. Our equation of state is a new functional form which has the property that the speed of sound approaches the speed of light in the limit of infinite compression. The equations of relativistic nuclear fluid dynamics are solved numerically in three spatial dimensions by use of a particle-in-cell finite-difference computing method for the reaction $^{20}Ne + ^{238}U$ at a laboratory bombarding energy per nucleon of 393 MeV. By integrating over the appropriate ranges of impact parameter, we compute the double-differential cross section $d^2\sigma/dEd\Omega$ corresponding both to all impact parameters and to central collisions constituting 15% of the total cross section. To within numerical uncertainties, the results for the various equations of state are very similar to one another except for central collisions at laboratory angle $\theta = 30°$ and for both central collisions and all impact parameters at $\theta = 150°$. In these cases, over certain ranges of energy, $d^2\sigma/dEd\Omega$ is larger for the density isomer than for conventional equations of state. The results calculated for all impact parameters are compared with the experimental data of Sandoval *et al.* for outgoing charged particles.

[NUCLEAR REACTIONS $^{20}Ne + ^{238}U$, $E_{lab}/20 = 393$ MeV; calculated $d^2\sigma/dEd\Omega$ for outgoing charged particles for all impact parameters and for central collisions. High-energy heavy-ion collisions, relativistic nuclear fluid dynamics, nuclear equation of state, density isomer, particle-in-cell finite-difference computing method.]

I. INTRODUCTION

With the development of accelerators that are capable of accelerating heavy nuclei to relativistic energies, we are now beginning to explore what happens when heavy nuclei become highly compressed and excited. As part of the theoretical effort in this area, several calculations of high-energy heavy-ion collisions have been performed on the basis of conventional nuclear fluid dynamics,[1-11] where the fundamental input is the nuclear equation of state. It is of crucial importance to know the sensitivity of the calculated results to the input equation of state.

Some two-dimensional and three-dimensional calculations have already been performed for different equations of state,[5-9] but the fairly large numerical errors that are present have precluded an accurate assessment of this sensitivity. In the present study we improve in two separate ways the numerical accuracy of three-dimensional relativistic nuclear fluid-dynamics calculations performed by use of a particle-in-cell finite-difference computing method.[1-5] First, we represent the fluid by approximately three times as many Lagrangian computational particles as were used previously. Second, we use an improved treatment of exterior cells that does not require setting their rest-frame density equal to normal nuclear density.

With this improved computing method, we study the effect of a density isomer in the nuclear equation of state, as well as the effect of varying the nuclear compressibility coefficient, on the distribution of outgoing matter in the reaction $^{20}Ne + ^{238}U$ at a laboratory bombarding energy per nucleon of 393 MeV. By integrating over the appropriate ranges of impact parameter, we compute the double-differential cross section $d^2\sigma/dEd\Omega$ corresponding both to all impact parameters and to central collisions constituting 15% of the total cross section. The results calculated for all impact parameters are compared with the recent experimental data of Sandoval *et al.* for outgoing charged particles.[12] Although we vary only the compressional contribution to the nuclear equation of state, an equally important problem for the future is to study the sensitivity of high-energy heavy-ion collisions to changes in the thermal contribution.

Our considerations are based on conventional nuclear fluid dynamics, which neglects any interpenetration that the target and projectile may experience upon contact. Although this interpenetration can be taken into account by means of two-fluid dynamics,[13] in which coupled relativistic equations of motion are solved for separate target

and projectile nuclear fluids, the effect of the equation of state in such a model has not been explored.

We introduce in Sec. II our nuclear equation of state, which is a new functional form with the property that the speed of sound approaches the speed of light in the limit of infinite compression. In Sec. III we discuss our relativistic fluid-dynamics equations of motion and the improvement that we have made in our particle-in-cell finite-difference computing method, which is used to calculate the time evolution of the matter distribution and the cross section $d^2\sigma/dEd\Omega$ for outgoing charged particles. Our conclusions are presented in Sec. IV.

II. NUCLEAR EQUATION OF STATE

The nuclear equation of state, which specifies how the pressure depends upon density and thermal energy, can be written as the sum of a contribution from the compressional energy and a contribution from the thermal energy. This is seen most clearly by recalling that the total internal energy per nucleon is given by [4]

$$\mathcal{E}(n,\mathcal{S}) = \mathcal{E}_0(n) + \mathcal{S} , \tag{1}$$

where $\mathcal{E}_0(n)$ is the ground-state energy per nucleon at nucleon number density n and $\mathcal{S}$ is the thermal energy per nucleon. The pressure p is then obtained from the fundamental relation[4]

$$p = n^2 \frac{\partial \mathcal{E}(n,\mathcal{S})}{\partial n}\bigg|_{\mathcal{S}} = n^2 \frac{d\mathcal{E}_0(n)}{dn} + n^2 \frac{\partial \mathcal{S}}{\partial n}\bigg|_{\mathcal{S}} , \tag{2}$$

with differentiation at constant entropy per nucleon $\mathcal{S}$.

A. Compressional contribution

For the ground-state energy per nucleon $\mathcal{E}_0(n)$ we use a new functional form which has the property that the speed of sound approaches the speed of light in the limit of infinite compression. This is achieved by parametrizing $\mathcal{E}_0(n)$ for n greater than a critical value n_a in terms of three smoothly joined parabolas in the density, so that in the limit of infinite compression it increases linearly with density. In the limit of zero density, $\mathcal{E}_0(n)$ is taken to be the difference between a specified term proportional to $n^{2/3}$ that represents the kinetic energy of noninteracting nucleons and a term proportional to n whose coefficient is adjusted so that the two forms join smoothly with continuous value and first derivative.

To be specific, our equation for $\mathcal{E}_0(n)$ is

$$\mathcal{E}_0(n) = \begin{cases} an^{2/3} - bn , & 0 \le n \le n_a , \\ \mathcal{E}_0(n_0) + \frac{2}{9}K_0\left[\left(\frac{n}{n_0}\right)^{1/2} - 1\right]^2 , & n_a \le n \le n_b , \\ \mathcal{E}_0(n_1) - \frac{2}{9}K_1\left[\left(\frac{n}{n_1}\right)^{1/2} - 1\right]^2 , & n_b \le n \le n_c , \\ \mathcal{E}_0(n_2) + \frac{2}{9}K_2\left[\left(\frac{n}{n_2}\right)^{1/2} - 1\right]^2 , & n_c \le n < \infty , \end{cases} \tag{3}$$

where

$$a = \frac{3}{10}\left(\frac{3\pi^2}{2}\right)^{2/3}\frac{\hbar^2}{m_0}$$

and m_0 is the nucleon mass. The quantity

$$K_i = (-1)^i 9 n_i^2 \frac{d^2\mathcal{E}_0}{dn^2}\bigg|_{n_i}$$

is the magnitude of the compressibility coefficient at equilibrium density n_i. We insert the factor $(-1)^i$ in its definition so that it is positive in each region. To adhere to standard notation, we often use the symbol $K \equiv K_0$ to refer to the compressibility coefficient at normal nucleon number density n_0. The quantity $\mathcal{E}_0(n_i)$ is the ground-state energy per nucleon at equilibrium density n_i.

In Eq. (3) for $\mathcal{E}_0(n)$ there appear three equilibrium densities n_i, three equilibrium energies $\mathcal{E}_0(n_i)$, three magnitudes of compressibility coefficients K_i, three joining points n_a, n_b, and n_c, and the coefficient b, resulting in a total of 13 constants. Six of these are eliminated by the requirement that $\mathcal{E}_0(n)$ be continuous in value and first derivative at the three joining points n_a, n_b, and n_c. This leaves a total of seven independent constants for the specification of $\mathcal{E}_0(n)$ when it contains a density isomer. For these seven constants we choose the equilibrium density, energy, and compressibility coefficient at normal density and at the density isomer, as well as the joining point n_b. By taking the limit in which n_b is infinite, we are also able to describe with Eq. (3) a conventional equation of state that does not contain a density isomer.

Once the seven independent constants n_0, $\mathcal{E}_0(n_0)$, K, n_2, $\mathcal{E}_0(n_2)$, K_2, and n_b have been specified, the joining points n_a and n_c, the coefficient b, the equilibrium density n_1, the energy $\mathcal{E}_0(n_1)$, and the compressibility coefficient K_1 are obtained by use of the formulas given in the Appendix.

We show in Fig. 1 the resulting ground-state energy $\mathcal{E}_0(n)$ for three specific choices of constants. In each case, normal nucleon number density

$$n_0 = \frac{1}{\frac{4\pi}{3}r_0^3}$$

is calculated with the value $r_0 = 1.18$ fm for the

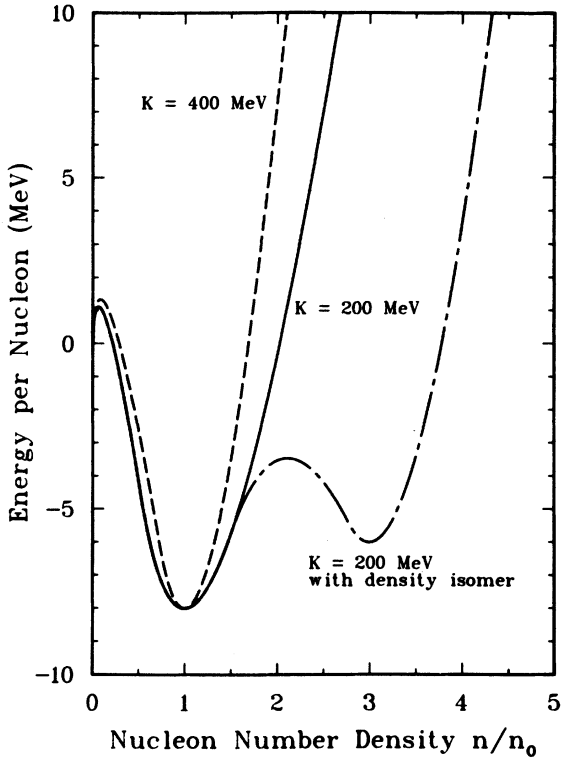

FIG. 1. Compressional contribution to our three nuclear equations of state.

fundamental nuclear-radius constant.[14] To simulate the effects of surface and Coulomb energies for finite nuclei, we use the value $\mathcal{E}_0(n_0) = -8$ MeV at normal nucleon number density.

The solid line in Fig. 1 shows the result for a conventional nuclear equation of state with compressibility coefficient $K = 200$ MeV, which is close to the experimental value of 210 ± 30 MeV deduced from experimental data on nuclear giant-monopole resonances.[15] The dashed line shows the effect of doubling the compressibility coefficient in a conventional nuclear equation of state to 400 MeV.

Finally, the dot-dashed curve in Fig. 1 shows the result for an equation of state with a density isomer that is taken to occur at a density $n_2 = 3\, n_0$ and an energy $\mathcal{E}_0(n_2) = -6$ MeV. The joining point is taken to be $n_b = \frac{3}{2}\, n_0$, below which the curve is taken to be identical to that for our conventional equation of state with $K = 200$ MeV. The compressibility coefficient for the density isomer is taken to be $K_2 = 1800$ MeV, so that the curvature at the density isomer is equal to that at normal density. The resulting curve is qualitatively similar to some that have been computed numerically by Migdal[16] and by Hecking and Weise,[17] who showed that pion condensation leads to a density isomer for certain values of their parameters.

B. Thermal contribution

For the thermal contribution to the pressure we use the nonrelativistic Fermi-gas model, which yields[4]

$$p_{\text{thermal}} = n^2 \left.\frac{\partial \mathcal{E}}{\partial n}\right|_s = \tfrac{2}{3} n \mathcal{E} . \tag{4}$$

Unlike what is often implied, this is a general result for the nonrelativistic Fermi-gas model that is valid to all orders in the temperature.

III. RELATIVISTIC FLUID DYNAMICS

A. Equations of motion

In a complete nuclear fluid-dynamics calculation, we would need to take into account surface energy, Coulomb energy, nuclear viscosity, thermal conductivity, and single-particle effects, as well as the production of additional particles and the associated radiative loss of energy from the system. However, in heavy-ion collisions at the laboratory bombarding energy per nucleon of 393 MeV considered here, these effects are small compared to those caused by the dominant kinetic, compressional, and thermal energies, and are consequently neglected.

The covariant relativistic hydrodynamic equations that we solve express the conservation of nucleon number, momentum, and energy for a specified nuclear equation of state. In units in which the speed of light $c = 1$, these equations are[1-4]

$$\frac{\partial N}{\partial t} + \nabla \cdot (\vec{v} N) = 0 , \tag{5a}$$

$$\frac{\partial \vec{M}}{\partial t} + \nabla \cdot (\vec{v} \vec{M}) = -\nabla p , \tag{5b}$$

and

$$\frac{\partial E}{\partial t} + \nabla \cdot (\vec{v} E) = -\nabla \cdot (\vec{v} p) , \tag{5c}$$

where N, $\vec{M}$, and E are, respectively, the nucleon number density, momentum density, and energy density (including rest energy) in the laboratory reference frame and $\vec{v}$ is the velocity of matter relative to the laboratory frame. The three laboratory-frame quantities are related to rest-frame quantities by

$$N = \gamma n , \tag{6a}$$

$$\vec{M} = \gamma^2 (\epsilon + p) \vec{v} , \tag{6b}$$

and

$$E=\gamma^2(\epsilon+p)-p\,, \tag{6c}$$

where $\gamma=(1-v^2)^{-1/2}$ and ϵ is the internal energy density in the rest frame, which is related to the internal energy per nucleon of Eq. (1) by

$$\epsilon=[m_0+\mathcal{E}(n,s)]n\,. \tag{7}$$

B. Particle-in-cell computing method

For our nuclear equation of state, which is specified by Eqs. (2)–(4), and for given initial conditions, we solve the equations of relativistic nuclear fluid dynamics numerically in three spatial dimensions by use of a particle-in-cell finite-difference computing method.[2] This technique is applicable to supersonic flow and combines some of the advantages of both Eulerian and Lagrangian methods. To facilitate comparisons with experimental results, the calculations are performed in the laboratory reference frame.

As in previous calculations with this technique, the computational mesh consists of fixed cubical Eulerian cells approximately 1.2 fm in length. The fluid, which moves through this mesh, is presented by about 26 000 discrete Lagrangian particles, corresponding to $3^3=27$ particles per cell for nuclear matter at equilibrium density. This is about three times the number of computational particles used previously.

From finite-difference representations of Eqs. (5), the values of N, $\vec{M}$, and E for each Eulerian cell are calculated at later times in terms of preceding values. The time step used for this purpose is approximately 2.8×10^{-24} s. By means of a partial algebraic reduction followed by the iterative solution of a transcendental equation in one unknown, Eqs. (2)–(4), (6), and (7) are solved to yield the values of n, $\vec{v}$, ϵ, and p throughout the mesh. Then the values of s can be found from Eqs. (1) and (7).

Another improvement in the present calculation concerns our treatment of exterior cells, for which the volume occupied by the fluid is in general less than the volume of the cell. In previous calculations, the rest-frame density of all exterior cells was simply set equal to equilibrium nuclear density.[2] Although this procedure is adequate during the early stages of the collision it becomes increasingly worse during the later expansion stage. We therefore determine the rest-frame density of edge cells by averaging the rest-frame densities of adjacent interior cells if there are any. For exterior cells that are not adjacent to interior cells, we compute the density by assuming that the entire cell volume is occupied by fluid.

C. Time evolution of the matter distribution

We consider the reaction ^{20}Ne + ^{238}U at a laboratory bombarding energy per nucleon of 393 MeV, for which there exist experimental data on the cross section $d^2\sigma/dEd\Omega$ for outgoing charged particles.[12] For each of the three equations of state illustrated in Fig. 1, we solve the equations of motion for five different impact parameters. We continue calculating the fluid-dynamical expansion to relatively small densities, where the thermal energy per nucleon is negligible, rather than perform a thermal folding after the system reaches a freezeout density at which fluid dynamics ceases to be valid.[18–20]

We show in Fig. 2 the calculated time evolution of the matter distribution for an impact parameter that is 0.1 the sum of the target and projectile radii, corresponding to nearly central collisions. Each column presents a side view of the matter distribution evolving in time for a different equation of state. The initial frame in each case shows a ^{238}U target bombarded from above by a Lorentz-contracted ^{20}Ne projectile whose energy per nucleon is 393 MeV. The projectile and target are represented by computational particles, which are initially aligned so that in the direction perpendicular to the page only a single point is visible. However, as the impulse resulting from the collision propagates throughout the system this alignment is destroyed and additional particles

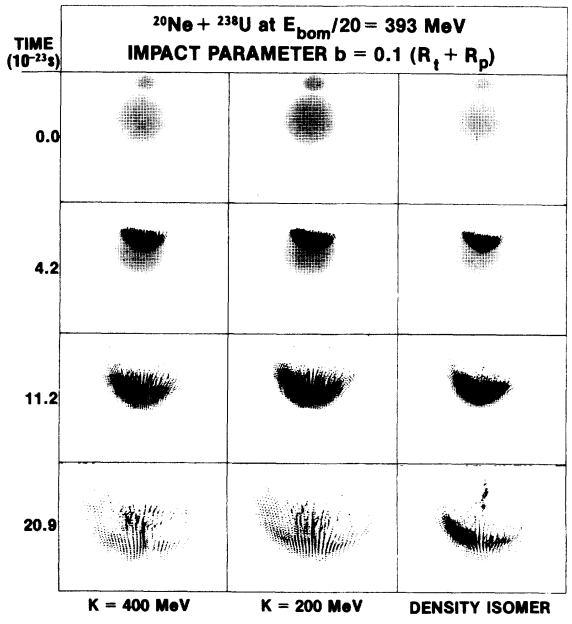

FIG. 2. Time evolution of the matter distribution in the collision of ^{20}Ne with ^{238}U, calculated for three different nuclear equations of state.

come into view.

The target and projectile are initially deformed, compressed, and excited by the collision, which produces curved shock waves.. These are followed by rarefaction waves and an overall expansion of the matter into a moderately wide distribution of angles. The results for the three different equations of state are very similar to one another, but the expansion stage starts later because the matter is compressed to a higher density for our equation of state with a density isomer compared to our two conventional equations of state.

Because it is difficult to extract densities from plots such as those in Fig. 2, we show in Fig. 3 perspective views of the rest-frame density in the midplane of the collision for our conventional equation of state with compressibility coefficient K = 200 MeV. In our finite-difference calculation, the matter is compressed to a maximum rest-frame density of 3.9 n_0. However, because of the rapid expansion of the system the rest-frame density remains above 2 n_0 for a total time of only 1.0×10^{-22} s. The calculated results for our other two equations of state are qualitatively similar to those shown in Fig. 3, although for our conventional equation of state with $K = 400$ MeV the matter is compressed to a maximum rest-frame density of only 3.4 n_0. For our equation of state with a density isomer the matter is compressed to a higher maximum rest-frame density of 5.1 n_0. In this case the rest-frame density remains above about 3 n_0 for a total time of 1.4×10^{-22} s and above 2 n_0 for a total time of 1.9×10^{-22} s.

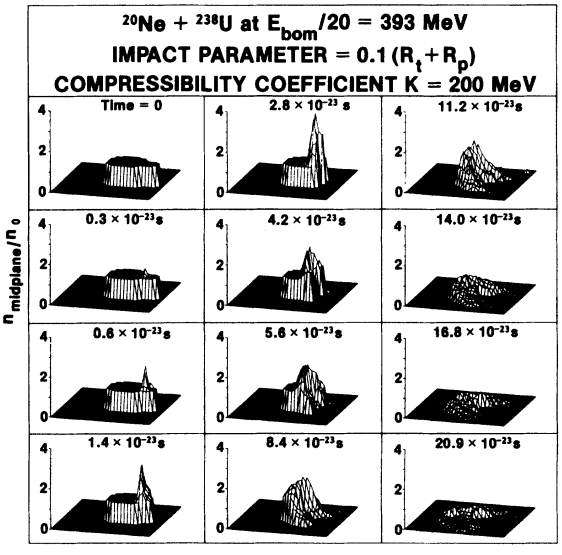

FIG. 3. Perspective views of the rest-frame density in the midplane of the collision of ^{20}Ne with ^{238}U, calculated for our conventional nuclear equation of state with compressibility coefficient $K = 200$ MeV.

D. Cross section $d^2\sigma/dEd\Omega$ for outgoing charged particles

For a given impact parameter we construct from the velocity vectors at some large time the energy and angular distributions for the expanding matter. The small amount of matter that already has passed through the top and side boundaries of the computational mesh is also included. By integrating over the appropriate ranges of impact parameter, we compute the double-differential cross section corresponding both to all impact parameters and to central collisions constituting 15% of the total cross section. The cross section for the outgoing matter distribution is then converted into the cross section $d^2\sigma/dEd\Omega$ for outgoing charged particles under the assumption of uniform charge density.

The results calculated for a conventional nuclear equation of state with compressibility coefficient $K = 200$ MeV are shown in Fig. 4 in the form of energy spectra at four laboratory angles ranging from 30° to 150°. Some measure of the numerical inaccuracies inherent in the calculations can be determined from the fluctuations in the histograms,

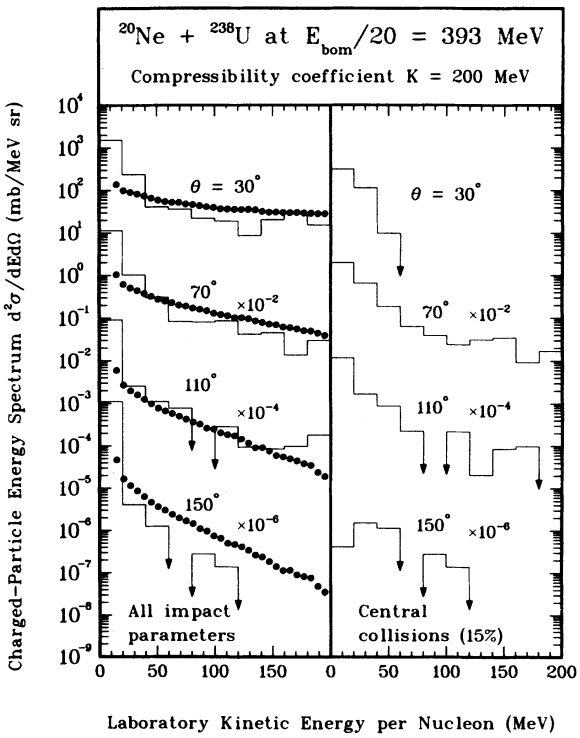

FIG. 4. Charged-particle energy spectrum $d^2\sigma/dEd\Omega$ calculated for our conventional nuclear equation of state with compressibility coefficient $K = 200$ MeV. The histograms calculated for all impact parameters are compared in the left-hand side of the figure with the experimental data of Sandoval *et al.* (Ref. 12).

which are obtained using angular bins of 10° width.

The results calculated for all impact parameters, given in the left-hand side of Fig. 4, are compared with the experimental data of Sandoval *et al.*[12] for outgoing charged particles, which include contributions from protons, deuterons, tritons, ^{3}He particles, and ^{4}He particles. Because of our neglect of binding, at low energy the calculated results at all angles are higher than the experimental results. At higher energy the calculations reproduce, to within numerical uncertainties, the experimental data at all angles except 150°, where the calculated results are somewhat below the experimental results.

The results calculated for central collisions constituting 15% of the total cross section are given in the right-hand side of Fig. 4. At low energy and all angles these results are significantly below those for all impact parameters. At laboratory angle $\theta = 30°$ the result for central collisions decreases much more rapidly with increasing energy than the result for all impact parameters. However, at $\theta = 150°$ the result for central collisions is at higher energy very similar to that for all impact parameters. We are unable to compare our calculations for central collisions with experimental data because the available data for central collisions do not yet include contributions from composite particles but instead include only protons.[21]

As shown in Fig. 5, the results calculated for a conventional nuclear equation of state with $K = 400$ MeV are very similar, to within numerical uncertainties, to those calculated with $K = 200$ MeV. Varying the compressibility coefficient alone in a conventional equation of state has little effect on the single-particle-inclusive cross section $d^2\sigma/dEd\Omega$ for either all impact parameters or central collisions. The insensitivity of the angular distribution to the compressibility coefficient has also been demonstrated by Bertsch and Amsden.[5]

We show finally in Fig. 6 the results calculated for our equation of state with a density isomer. At most energies and angles these results are very similar, to within numerical uncertainties, to those calculated for conventional equations of state. However, for central collisions at $\theta = 30°$ the results calculated for a density isomer decrease more slowly with increasing energy than those calculated for conventional equations of state.

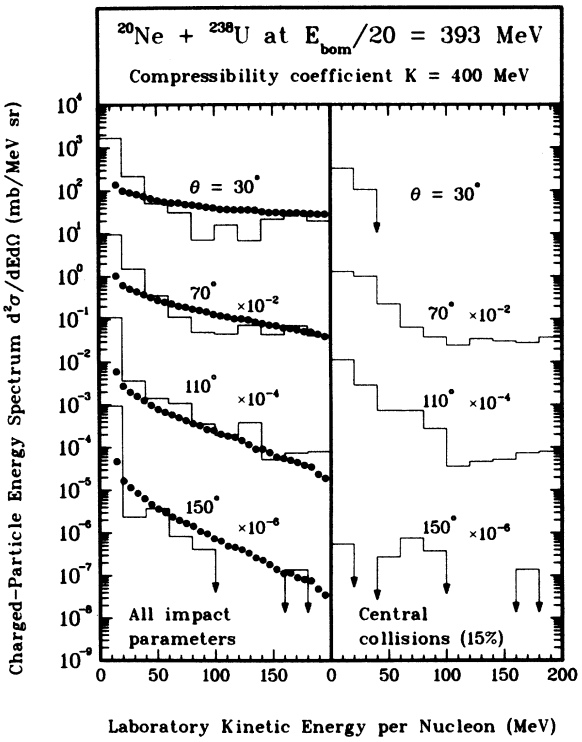

FIG. 5. Charged-particle energy spectrum $d^2\sigma/dEd\Omega$ calculated for our conventional nuclear equation of state with compressibility coefficient $K = 400$ MeV. The histograms calculated for all impact parameters are compared in the left-hand side of the figure with the experimental data of Sandoval *et al.* (Ref. 12).

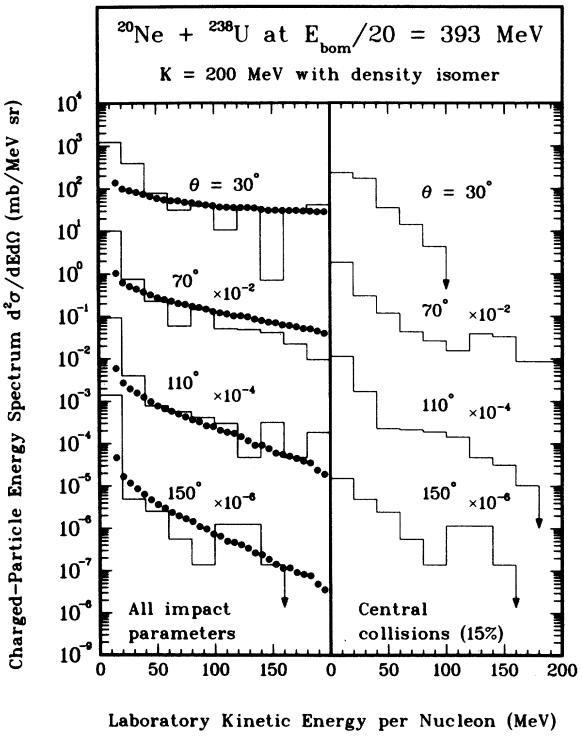

FIG. 6. Charged-particle energy spectrum $d^2\sigma/dEd\Omega$ calculated for our nuclear equation of state with a density isomer. The histograms calculated for all impact parameters are compared in the left-hand side of the figure with the experimental data of Sandoval *et al.* (Ref. 12).

Also, for both central collisions and all impact parameters at $\theta = 150°$ the results calculated for the density isomer are higher than those calculated for conventional equations of state. These differences arise because at this bombarding energy the softer density-isomer equation of state leads to higher initial density and thermal energy per nucleon, which increases the thermal contribution to the cross section in regions where it would otherwise be small.

E. Errors

Several sources of errors in the numerical method used in this paper to solve the relativistic Euler equations have been identified. Among these are the finite time step, the finite cell size, the finite number of marker particles and their original placement, the treatment of edge cells and round off errors.

The magnitude of the errors is difficult to assess. However, one advantage of the particle-in-cell method is that one may obtain an estimate of the *statistical* error: If the number of marker particles in an energy-angle bin is N, the statistical error is $\sqrt{N}$. One may then relate this to a statistical error in the calculated $d^2\sigma/dEd\Omega$. The resulting errors are shown in Fig. 7 for the equation of state having a compressibility of $K = 200$ MeV. The statistical errors for the other two equations of state are similar and are not shown.

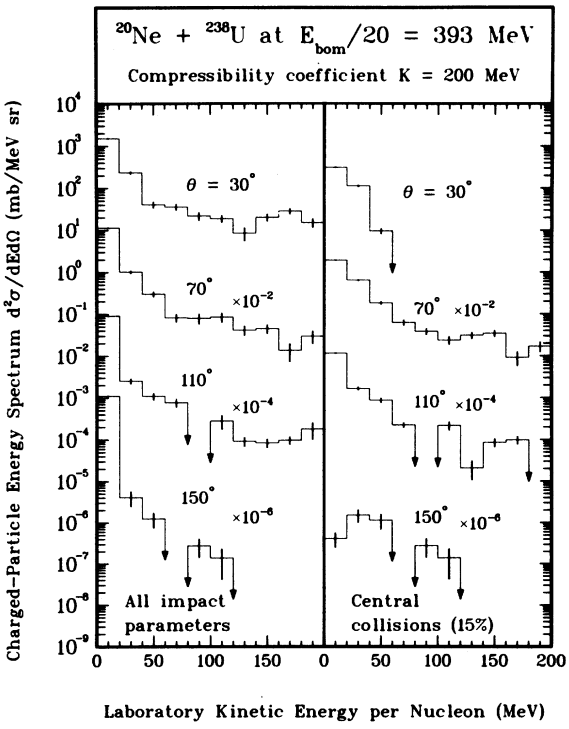

FIG. 7. Charged-particle energy spectrum $d^2\sigma/dEd\Omega$ calculated for our conventional nuclear equation of state with compressibility coefficient $K = 200$ MeV. The error bars represent the calculated statistical errors.

Errors induced by using a finite time step were investigated by performing several calculations using different time steps; the resultant errors were less than the statistical errors for time steps less than 5.6×10^{-24}s or twice the time step actually employed. The principal effect of using a shorter time step was to reduce fluctuations in the rest frame density and the entropy. The effects of finite cells and the finite number of marker particles were investigated in a similar fashion subject to the constraint of available computer memory. The calculations described in the previous sections used 12 cells to span the ^{238}U nucleus. Decreasing the number of cells to 10 produced a double differential cross section with larger relative errors, but which encompassed the previous $d^2\sigma/dEd\Omega$ calculated with 12 cells. Decreasing the number of cells to eight produced large numerical fluctuations. By increasing the amount of volume within the computational mesh occupied by the two nuclei, it was possible to perform a calculation in which 16 cells spanned the ^{238}U nucleus. Although the reaction could be meaningfully followed for only a few time steps before large numbers of marker particles began to leave the mesh, the calculated maximum density differed from the calculation employing 12 cells by less than 10 percent.

The original placement of the marker particles was at the vertices of a closely packed cubic array. The marker particles were 0.4 fm apart. This regular spacing gives rise in part to the striations evident in Fig. 3. Effects of this regular placement of the marker particles were investigated by randomly placing the marker particles in a sphere of radius 0.04 fm centered about its original position. The principal result of this randomization was to reduce the amount of apparent striation, but again the effect on the calculated $d^2\sigma/dEd\Omega$ was less than the statistical error.

Two further important checks were performed. After each cycle of the calculation, the total momentum, energy, and entropy was calculated. The energy and each Cartesian component of momentum were conserved to a relative accuracy of 10^{-14}. To save computer storage the positions of each of the computational particles were stored in one half of a 60 bit word; no loss of precision was found and the effects of round off error were therefore adjudged to be insignificant. Finally, the expansion of the nuclear fluid should be isentropic after the creation of the shock wave. In the calculations reported here, the entropy initially in-

creased rapidly, but approximately 5×10^{-23} s after the initiation of the reaction, the calculated entropy remained constant with fluctuations of 5%.

IV. CONCLUSIONS

On the basis of a three-dimensional relativistic nuclear fluid-dynamics calculation of the single-particle-inclusive cross section $d^2\sigma/dEd\Omega$ for all impact parameters and for central collisions, we have shown that the calculated results depend very little on the nuclear compressibility coefficient. Thermal folding after freezeout would reduce the small differences that are present even further.

A strong density isomer increases the cross section $d^2\sigma/dEd\Omega$ for central collisions at $\theta=30°$ and for both central collisions and all impact parameters at $\theta=150°$, but numerical uncertainties are comparable to the effect. Furthermore, the inclusion of transparency in a more realistic model that goes beyond conventional nuclear fluid dynamics would also increase $d^2\sigma/dEd\Omega$ for central collisions at $\theta=30°$, which complicates the interpretation of experimental data.

Although current experimental data on relativistic heavy-ion collisions can be understood on the basis of conventional ideas, the work done thus far provides a necessary background for the identification of any new phenomena that may result from high compression and excitation of nuclear matter. Possible directions for the future include studies of excitation functions, two-particle correlations, impact-parameter dependences, particle-multiplicity distributions, the deuteron/proton ratio, and the Coulomb distortion of charged-pion spectra.

ACKNOWLEDGMENTS

We are grateful to A. A. Amsden and F. H. Harlow for their participation in the early states of this work, to A. J. Sierk for helping us check the equations in the Appendix, and to J. I. Kapusta, J. W. Negele, and A. J. Sierk for stimulating discussions. This work was supported by the U. S. Department of Energy.

APPENDIX: DETERMINATION OF DEPENDENT CONSTANTS IN THE EQUATION FOR $E_0(n)$

We give here the formulas that permit the calculation of the six dependent constants in Eq. (3) in terms of the seven independent constants. The requirement that $E_0(n)$ be continuous in value and first derivative at the joining point n_a gives two equations involving the two unknown quantities n_a and b. A small amount of algebra yields the equation

$$\tfrac{1}{3}an_a^{2/3}+\frac{2}{9}\frac{K}{n_0^{1/2}}n_a^{1/2}-[\mathcal{E}_0(n_0)+\tfrac{2}{9}K]=0\,,$$

which is solved iteratively by use of Newton's method for the intersection point n_a. The coefficient b is then given by

$$b=\frac{2}{3}\frac{a}{n_a^{1/3}}+\frac{2}{9}K\left[\frac{1}{(n_an_0)^{1/2}}-\frac{1}{n_0}\right].$$

The requirement that $\mathcal{E}_0(n)$ be continuous in value and first derivative at the intersection point n_b yields one equation involving the three unknown quantities, n_1, $\mathcal{E}_0(n_1)$, and K_1 and a second equation involving n_1 and K_1. A similar requirement at the joining point n_c yields one equation involving the four unknown quantities n_1, $\mathcal{E}_0(n_1)$, K_1, and n_c and a second equation involving n_1, K_1, and n_c. After a considerable amount of algebra, we are able to obtain the joining point n_c from the equation

$$\left(\frac{n_c}{n_0}\right)^{1/2}=\left(\frac{n_2}{n_0}\right)^{1/2}-\frac{\left[\left(\frac{n_b}{n_0}\right)^{1/2}-1\right]\left[\left(\frac{n_2}{n_0}\right)^{1/2}-1\right]+\frac{9}{2}[\mathcal{E}_0(n_0)-\mathcal{E}_0(n_2)]/K}{\left(\frac{n_b}{n_0}\right)^{1/2}-1+\left[\left(\frac{n_2}{n_0}\right)^{1/2}-\left(\frac{n_b}{n_0}\right)^{1/2}\right]\frac{n_0}{n_2}\frac{K_2}{K}}$$

The equilibrium energy $\mathcal{E}_0(n_1)$ is then given by

$$\mathcal{E}_0(n_1)=\mathcal{E}_0(n_2)+\frac{2}{9}\frac{\left[\left(\frac{n_2}{n_0}\right)^{1/2}-\left(\frac{n_c}{n_0}\right)^{1/2}\right]^2\left(\frac{n_0}{n_2}\right)^2\frac{K_2^2}{K}}{\left(\frac{n_b}{n_0}\right)^{1/2}-1+\left[\left(\frac{n_2}{n_0}\right)^{1/2}-\left(\frac{n_c}{n_0}\right)^{1/2}\right]\frac{n_0}{n_2}\frac{K_2}{K}}\left[\frac{\left(\frac{n_b}{n_0}\right)^{1/2}-1}{\frac{n_0}{n_2}\frac{K_2}{K}}+\left(\frac{n_2}{n_0}\right)^{1/2}-\left(\frac{n_b}{n_0}\right)^{1/2}\right],$$

in terms of which the equilibrium density n_1 is obtained from

$$\left(\frac{n_1}{n_0}\right)^{1/2}=\left(\frac{n_b}{n_0}\right)^{1/2}+\frac{\left[\left(\frac{n_b}{n_0}\right)^{1/2}-1\right]\left\{\frac{9}{2}[\mathcal{E}_0(n_1)-\mathcal{E}_0(n_2)]/K-\left[\left(\frac{n_2}{n_0}\right)^{1/2}-\left(\frac{n_c}{n_0}\right)^{1/2}\right]^2\right\}}{\left[\left(\frac{n_2}{n_0}\right)^{1/2}-\left(\frac{n_c}{n_0}\right)^{1/2}\right]^2\left(\frac{n_0}{n_2}\right)^2\left(\frac{K_2}{K}\right)^2}.$$

The compressibility coefficient K_1 is given finally by

$$K_1=\frac{\left[\left(\frac{n_b}{n_0}\right)^{1/2}-1\right]\frac{n_1}{n_0}}{\left[\left(\frac{n_1}{n_0}\right)^{1/2}-\left(\frac{n_b}{n_0}\right)^{1/2}\right]}K.$$

[1]A. A. Amsden, G. F. Bertsch, F. H. Harlow, and J. R. Nix, Phys. Rev. Lett. 35, 905 (1975).

[2]F. H. Harlow, A. A. Amsden, and J. R. Nix, J. Comput. Phys. 20, 119 (1976).

[3]A. A. Amsden, F. H. Harlow, and J. R. Nix, Phys. Rev. C 15, 2059 (1977).

[4]J. R. Nix, Prog. Part. Nucl. Phys. 2, 237 (1979).

[5]G. F. Bertsch and A. A. Amsden, Phys. Rev. C 18, 1293 (1978).

[6]H. Stöcker, J. A. Maruhn, and W. Greiner, Z. Phys. A 290, 297 (1979).

[7]H. Stöcker, J. A. Maruhn, and W. Greiner, Z. Phys. A 293, 173 (1979).

[8]H. Stöcker, R. Y. Cusson, J. A. Maruhn, and W. Greiner, Z. Phys. A 294, 125 (1980).

[9]P. Danielewicz, Nucl. Phys. A314, 465 (1979).

[10]L. P. Csernai, H. W. Barz, B. Lukács, and J. Zimányi, in *Proceedings of the EPS Topical Conference on Large Amplitude Collective Nuclear Motions, Keszthely, Hungary, 1979* (Central Research Institute for Physics, Budapest, 1979), Vol. II, p. 533.

[11]H. H. K. Tang and C. Y. Wong, Phys. Rev. C 21, 1846 (1980).

[12]A. Sandoval, H. H. Gutbrod, W. G. Meyer, R. Stock, C. Lukner, A. M. Poskanzer, J. Gosset, J. C. Jourdain, C. H. King, G. King, V. S. Nguyen, G. D. Westfall, and K. L. Wolf, Phys. Rev. C 21, 1321 (1980).

[13]A. A. Amsden, A. S. Goldhaber, F. H. Harlow, and J. R. Nix, Phys. Rev. C 17, 2080 (1978).

[14]W. D. Myers, At. Data Nucl. Data Tables 17, 411 (1976).

[15]J. P. Blaizot, D. Gogny, and B. Grammaticos, Nucl. Phys. A265, 315 (1976).

[16]A. B. Migdal, Rev. Mod. Phys. 50, 107 (1978).

[17]P. Hecking and W. Weise, Phys. Rev. C 20, 1074 (1979).

[18]A. Mekjian, Phys. Rev. Lett. 38, 640 (1977).

[19]R. Bond, P. J. Johansen, S. E. Koonin, and S. Garpman, Phys. Lett. 71B, 43 (1977).

[20]J. I. Kapusta, Phys. Rev. C 16, 1493 (1977).

[21]R. Stock, H. H. Gutbrod, W. G. Meyer, A. M. Poskanzer, A. Sandoval, J. Gosset, C. H. King, G. King, C. Lukner, V. S. Nguyen, G. D. Westfall, and K. L. Wolf, Phys. Rev. Lett. 44, 1243 (1980).

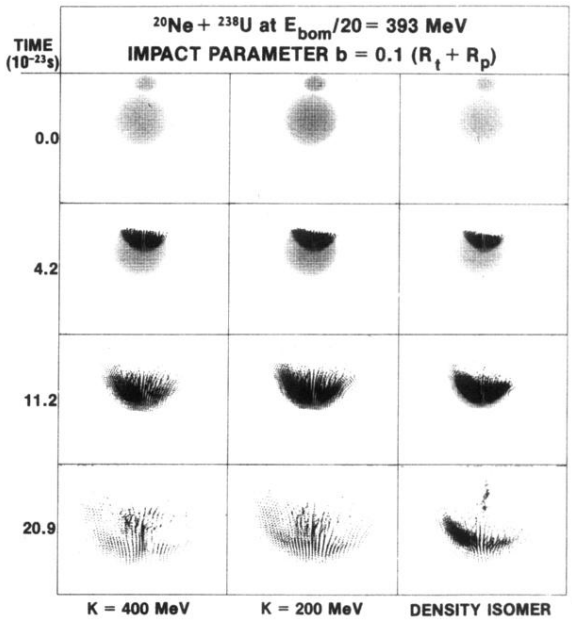

FIG. 2. Time evolution of the matter distribution in the collision of ^{20}Ne with ^{238}U, calculated for three different nuclear equations of state.